SFM-MVS to Mesh

Roderick Lan
1706751

Abdullah Khadelli
1722102

***Abstract*—Structure From Motion (SFM) and Multiview Stereo (MVS) are computer vision algorithms commonly found in a wide range of domains and use cases, one of the most prevalent being photogrammetry. In this project, we investigate the ideal methodology and object properties for photogrammetry of specific objects using SFM, and explore an altered approach to the feature extraction and feature matching steps in the algorithm. Additionally, we evaluate the effectiveness of two algorithms for surface reconstruction on our SFM-MVS (point cloud) outputs.**

1. Introduction

One of the most common applications of Structure From Motion (SFM) and Multiview Stereo (MVS) is in photogrammetry. These two techniques are complementary to each other, and result in a dense point cloud reconstruction of an object (or environment) from image data. However, in many fields where photogrammetry is used, a 3D mesh is likely more useful than a point cloud is. As such, time is often spent cleaning resultant point clouds and converting them to meshes, when the brunt of this process could be automated and simplified. Furthermore, SFM can be relatively slow for many datasets. The general outline of SFM algorithms involves feature extraction, feature matching, triangulation and bundle adjustment. Each of these steps can take considerable time, however there is not much to change with regards to triangulation and bundle adjustment. On the other hand, feature extraction (SIFT [1] based) and feature matching can be altered to be computationally faster at a minimal cost to accuracy. In a nutshell, this project report will explore proposed alterations to feature extraction and feature matching in SFM, investigate the ideal methodologies and object types for this altered approach, and evaluate algorithms relating to point cloud processing and mesh reconstruction. The source code for the project can be found on GitHub.

2. Theory and Technical Details

This project largely focuses on alterations to SFM and post processing SFM-MVS output for mesh construction. The general workflow and steps taken in this project can be seen in Figure 1.

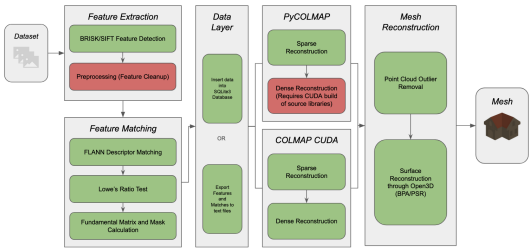

Figure 1. Pipeline/Project Workflow

2.1. SFM-MVS

SFM algorithms generally consist of the following steps: feature extraction, feature matching, triangulation, and bundle adjustment.
Traditionally, feature extraction in SFM algorithms use Lowe's SIFT approach for both feature detection and description [1]. Detection in SIFT involves a Gaussian pyramid-like structure of octaves for scale space representation. Each octave of scale space contains a set of Gaussian convolved images separated by a scale factor, and each octave uses a down-sampled image relative to the previous octave. The extrema (within a given window) of a difference-of-Gaussian (DoG) (Figure 2) function applied to adjacent Gaussian images within octaves is used to detect stable key points in scale space. Mathematically, the scale space is defined as a function $L(x, y, \sigma)$, produced from a variable-scale Gaussian, $G(x, y, \sigma)$ and the input image $I(x, y)$ [1]:

$$L(x, y, \sigma) = G(x, y, \sigma) * I(x, y)$$

where $*$ is the convolution operation. The DoG function takes the form:

$$\begin{aligned} D(x, y, \sigma) &= (G(x, y, k\sigma) - G(x, y, \sigma)) * I(x, y) \\ &= L(x, y, k\sigma) - L(x, y, \sigma) \end{aligned}$$

with some constant multiplicative scale factor k. DoG approximates the normalized Laplacian of Gaussian [2] , whose local extrema was shown to correspond to stable key points/blobs. SIFT descriptors [1] take the gradient directions over a spatial region around feature points. A histogram of these gradient directions (orientations) is normalized and invariant against rotation, scale, and brightness.

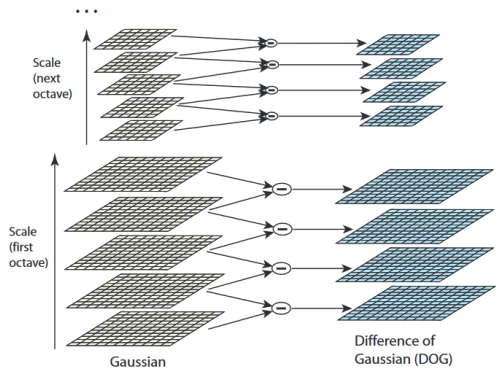

Figure 2. Difference of Gaussians and Sift Scale Space
Source: Adapted from [1]

The descriptors are stored as a 128-dimensional vector containing these histogram values corresponding to the gradient magnitudes and are known for their distinctiveness. BRISK feature detection [3] builds on a computationally optimized version of FAST 9-16 adapted for scale invariance via a simplified representation of scale space (compared to SIFT [1]). Due to the simplified scale space representation and use of a computationally efficient FAST 9-16 detection algorithm, BRISK is considerably faster than SIFT while still detecting high quality key points. The set of detected points with BRISK is similar to many SIFT detected points. Additionally, since both approaches revolve around scale, rotation, and illuminance invariance, and since description is independent of detection, SIFT descriptors can be easily applied to BRISK key points. For the purposes of this project, we rely on OpenCV's implementation of both SIFT [4] and BRISK [5]. Feature matching in SFM (with SIFT descriptors) is done by identifying a nearest neighbor (based on L2 distance) between descriptors in 2 views [1]. This is efficiently approximated through [6].
Lowe's ratio test [1] compares the distance measures of the 2 nearest neighbors and rejects matches where the ratio between the distances from these neighbors is greater than or equal to some value l (ie. $d_1 \geq l \cdot d_2$), eliminating false matches. [7]'s MAGSAC++ [8], an improved version of RANSAC, further refines these matches by finding inliers during a fundamental matrix estimation between randomly sampled matches. Two view geometry estimation, triangulation and bundle adjustment, as well as multiview stereo, are handled through COLMAP [9] [10] [11], resulting in sparse and dense point cloud reconstructions (with estimated surface normals).

2.2. Feature Preprocessing

During feature extraction, further processing can be done to isolate key points on objects. We apply a combination of image filtering, blurring, and canny edge detection to build a binary mask (show in Figure 3) covering the object of interest. This mask is used to discard key points which

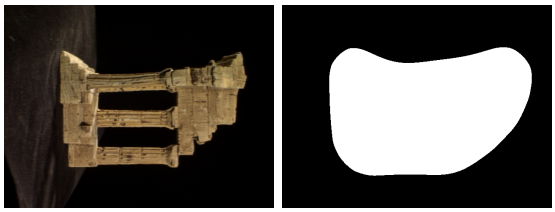

(a) Initial Image (b) Binary mask

Figure 3. Binary Mask

are determined to be background noise. Preparation for canny edge detection involves noise reduction through a gaussian blur for effective detection [12]. Though OpenCV's implementation [13] applies a 5×5 Gaussian kernel, further reduction is often necessary. Additionally, we apply a DoG (shown in Figure 4) based approach to accentuate edges and blobs for lower texture objects and noisier datasets. Sobel

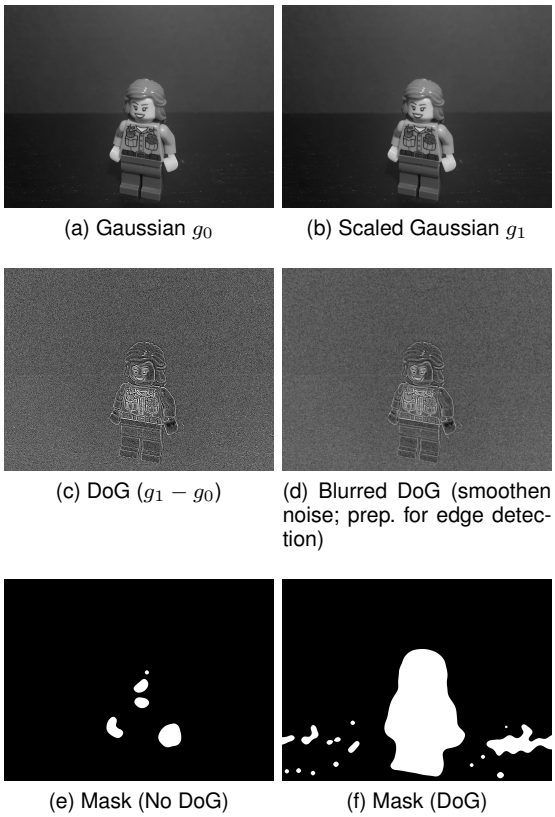

(a) Gaussian g_0 (b) Scaled Gaussian g_1

(c) DoG ($g_1 - g_0$) (d) Blurred DoG (smoothen noise; prep. for edge detection)

(e) Mask (No DoG) (f) Mask (DoG)

Figure 4. Difference of Gaussian based preprocessing approach. (σ-scale factor $k = 2$) Inspired by [1].

filters applied in the horizontal and vertical directions allow us to obtain edge gradients and directions [13] as follows:

$$G = \sqrt{G_x^2 + G_y^2}, \quad \theta = \arctan\left(\frac{G_y}{G_x}\right)$$

where G is the edge gradient and θ is the edge direction. Non-maximum suppression removes unwanted pixels that

may not be part of an edge []. Hystersis thresholding determines edge criterion via a user defined lower-upper bound (l, u):

i $G > u \rightarrow$ edge
ii $G < l \rightarrow$ not an edge
iii $G \in [l, u] \rightarrow$ classified based on connectivity to edge pixels

We use the edge image, $E(x, y)$, to build a mask by:

1. Convolving a Gaussian kernel on E
2. Binary thresholding is applied to the convolved image (forming the initial mask M)
3. Apply two median blur filters to M

We can apply our mask to the source frame and exclude key points that are irrelevant to the image. Though this does not directly affect the dense point cloud reconstruction from MVS, it can decrease matches from background noise, thus improving match performance and the accuracy of two view geometry. A general outline of our feature preprocessing approach is shown in Figure 5 and an example is how in Figure 6

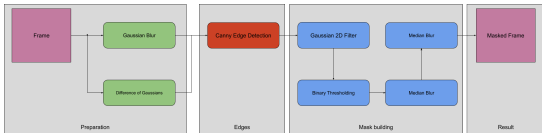

Figure 5. Feature preprocessing pipeline

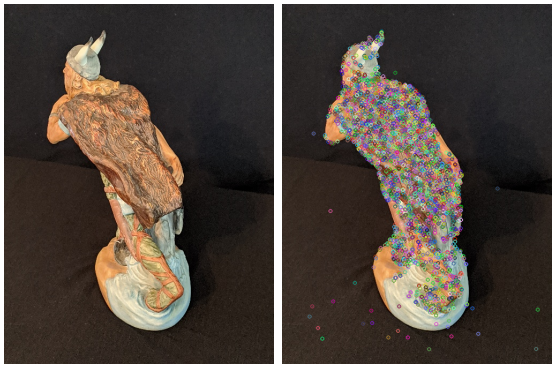

(a) Source Image (b) BRISK keypoints

(c) Edge (d) Mask (e) Masked image

Figure 6. Feature preprocessing example

2.3. Point Cloud Processing

This project uses Open3D's implementation of the Ball-Pivot Algorithm (BPA) [14] [15] and Poisson Surface Reconstruction (PSR) [16] [15], two widely used mesh reconstruction techniques. BPA involves a "ball" with a user-defined radius, r, which pivots along a manifold surface of the 3D object. Triangles are formed when the ball touches 3 points without "falling through", eventually leading to a triangle mesh once all points are considered [14]. This process can be repeated with various different radii to improve accuracy. An implementation trick we discovered with radii tuning was defining them as an array of scaled average neighbor distances. This approach often gave the best results with respect to BPA. PSR [16] formalizes surface reconstruction as a poisson problem and creates very smooth surfaces that robustly approximate noisy data using a point cloud, its normals, and an octree of a user specified depth. However, PSR assumes the point cloud represents an object rather than the environment surrounding it, as such its robustness to noise is limited when background points are introduced. Additionally, BPA [14] is generally not as robust as PSR for noise in an object point cloud, however it handles background noise well (given enough separation between points). To alleviate the effect of noise, we use Open3D's radial and statistical point cloud outlier removal algorithms to automate background noise removal [17], improving overall mesh quality for both approaches.

3. Results

(a) SIFT Features (b) BRISK Features

Figure 7. SIFT vs BRISK detected features

References

[1] D. G. Lowe, "Distinctive image features from scale-invariant keypoints," *International journal of computer vision*, vol. 60, pp. 91–110, 2004.

[2] T. Lindeberg, "Feature detection with automatic scale selection," *International journal of computer vision*, vol. 30, pp. 79–116, 1998.

[3] S. Leutenegger, M. Chli, and R. Y. Siegwart, "Brisk: Binary robust invariant scalable keypoints," in *2011 International Conference on Computer Vision*, 2011, pp. 2548–2555.

[4] "Opencv: cv::sift class reference," docs.opencv.org. [Online]. Available: https://docs.opencv.org/4.x/d7/d60/classcv_1_1SIFT.html

[5] "Opencv: cv::brisk class reference," docs.opencv.org. [Online]. Available: https://docs.opencv.org/4.x/de/dbf/classcv_1_1BRISK.html

[6] “Opencv: cv::flannbasedmatcher class reference,” docs.opencv.org. [Online]. Available: https://docs.opencv.org/3.4/dc/de2/classcv_1_1FlannBasedMatcher.html

[7] “Opencv: Usac: Improvement of random sample consensus in opencv,” docs.opencv.org. [Online]. Available: https://docs.opencv.org/4.x/de/d3e/tutorial_usac.html

[8] D. Barath, J. Noskova, M. Ivashechkin, and J. Matas, “Magsac++, a fast, reliable and accurate robust estimator,” 2019.

[9] “Colmap,” https://github.com/colmap/colmap, 2024.

[10] J. L. Schönberger and J.-M. Frahm, “Structure-from-motion revisited,” in *Conference on Computer Vision and Pattern Recognition (CVPR)*, 2016.

[11] J. L. Schönberger, E. Zheng, M. Pollefeys, and J.-M. Frahm, “Pixelwise view selection for unstructured multi-view stereo,” in *European Conference on Computer Vision (ECCV)*, 2016.

[12] J. Canny, “A computational approach to edge detection,” *IEEE Transactions on Pattern Analysis and Machine Intelligence*, vol. PAMI-8, no. 6, pp. 679–698, 1986.

[13] “Canny edge detection,” docs.opencv.org. [Online]. Available: https://docs.opencv.org/4.x/da/d22/tutorial_py_canny.html

[14] F. Bernardini, J. Mittleman, H. Rushmeier, C. Silva, and G. Taubin, “The ball-pivoting algorithm for surface reconstruction,” *IEEE Transactions on Visualization and Computer Graphics*, vol. 5, no. 4, pp. 349–359, 1999.

[15] “Surface reconstruction - open3d 0.18.0 documentation,” www.open3d.org. [Online]. Available: https://www.open3d.org/docs/release/tutorial/geometry/surface_reconstruction.html

[16] M. Kazhdan, M. Bolitho, and H. Hoppe, “Poisson surface reconstruction,” in *Proceedings of the fourth Eurographics symposium on Geometry processing*, vol. 7, no. 4, 2006.

[17] “Point cloud outlier removal — open3d 0.9.0 documentation,” www.open3d.org. [Online]. Available: https://www.open3d.org/docs/0.9.0/tutorial/Advanced/pointcloud_outlier_removal.html